ICES Journal of Marine Science

ICES Journal of Marine Science (2016), 73(10), 2729–2736. doi:10.1093/icesjms/fsw110

Original Article

Improving the estimations of transect length and width for underwater visual surveys of targets on or near the seabed

Kevin L. Stierhoff*, David W. Murfin, David A. Demer, Scott A. Mau, and Deanna R. Pinkard-Meier‡

Fisheries Resources Division, National Marine Fisheries Service, Southwest Fisheries Science Center, 8901 La Jolla Shores Dr, La Jolla, CA 92037, USA

**Corresponding author: tel: +858 546 7180; fax: +858 546 5651; e-mail: kevin.stierhoff@noaa.gov.*

‡*Present address: Biology Department, University of San Diego, 5998 Alcala Park Dr., San Diego, CA, 92110, USA.*

Stierhoff, K. L., Murfin D. W., Demer, D. A., Mau, S. A., and Pinkard-Meier, D. R. Improving the estimations of transect length and width for underwater visual surveys of targets on or near the seabed. – ICES Journal of Marine Science, 73: 2729–2736.

Received 10 November 2015; revised 26 May 2016; accepted 29 May 2016; advance access publication 10 July 2016.

Demersal marine organisms may be surveyed visually using cameras deployed on a submersible vehicle, e.g. a remotely operated vehicle (ROV). For estimating animal densities along visual transects, the sampled area may be calculated from the products of transect distance and width. In this study, distance was measured relative to submerged pipeline features of known length using: 1) speed estimates from a Doppler velocity log (DVL); and 2) position estimates from an ultra-short baseline (USBL) acoustic system. DVL estimates of distance were within 0.8 to 1.0% of known feature lengths ranging from 6.01 to 1520.53 m, respectively. USBL estimates of distance were less accurate, ranging from 3.2 to 5.0% over the same distances, and positively biased compared to DVL estimates. Also, transect-width estimates were compared using: 1) calibrated laser metrics; and 2) measurement of camera orientation and optical properties. Both methods produced similar estimates of transect width, and thus area ($r^2 = 0.81$), but width varied with camera altitude and orientation, and increased with seabed relief. Therefore, an assumption of constant transect width may bias estimates of sampled area, and estimates of animal density and abundance, particularly when surveying over seabeds with variable relief. To minimize these biases, practical methods are described to quantify transect distance and width throughout surveys using standard survey equipment and analytical methods.

Keywords: laser projection, photogrammetry, population assessment, remotely operated vehicle, video.

Introduction

Benthic trawls are routinely used to monitor the distribution, abundance, and length composition of groundfishes off the U.S. West Coast (Keller *et al.*, 2006, 2007), but may not effectively sample organisms, such as rockfishes (genus *Sebastes*) that have a strong affinity for high-relief rocky substrates (Jagielo *et al.*, 2003), or may be prohibited in closed areas, for example in the Cowcod Conservation Areas (CCAs) off the coast of southern California (CA). Rockfishes may be surveyed using SCUBA, unless depth and time restrictions make that approach impractical. In such cases, visual surveys may be conducted using cameras deployed from submerged vehicles, including: remotely operated vehicles (ROVs), human-occupied submersibles, and autonomous underwater vehicles. Relative to trawl sampling, visual surveys: i) are less destructive to sensitive benthic habitats; ii) do not negatively impact or extract rare or endangered organisms; and iii) provide information on the behaviours of target organisms and their associations with certain seabed features. Visual surveys have provided estimates of abundance and density of multiple benthic and demersal species (Adams *et al.*, 1995), including population estimates of depleted rockfishes in untrawlable habitats (Yoklavich *et al.*, 2007) and endangered white abalone (*Haliotis sorenseni*) that inhabit deep, offshore rocky reefs (Stierhoff *et al.*, 2012).

Visual surveys are often conducted using the strip-transect method (Buckland *et al.*, 2001), an extension of classical quadrat sampling, which requires accurate estimates of the sampled area calculated from the products of estimated transect distance and width. Errors associated with estimates of transect length and width contribute directly to errors in the estimates of animal density and abundance and may degrade the ability of survey results

to inform assessments of exploited stocks or the recovery status of threatened or endangered species.

Transect length may be estimated from: i) the summed, incremental distance between dots on the seabed from a laser caliper (i.e., paired parallel lasers with known spacing) (Yoklavich *et al.*, 2000), ii) the sum of Euclidian distances between sequential filtered and smoothed estimates of the geographic position from an ultra-short baseline acoustic positioning system (USBL) (Pinkard *et al.*, 2005; Yoklavich *et al.*, 2007), iii) precise and frequent measurements of time and speed from a Doppler velocity log (DVL), or iv) using a combination of data from USBL and DVL systems, perhaps smoothed with a Kalman filter (Kalman, 1960). Often, methods used to estimate transect length are not calibrated, e.g. by comparing and adjusting results relative to a known distance (e.g., Adams *et al.*, 1995; O'Connell and Carlile, 1993; Yoklavich *et al.*, 2000, 2007). A USBL system may be adjusted to minimize systematic positioning errors resulting from sensor misalignment (i.e., pitch, roll and heading) and variations in sound velocity (Opderbecke, 1997).

Transect width varies with camera pitch (i.e., elevation angle relative to horizontal defining rotation in the fore-aft plane), altitude (i.e., height of the camera above the seabed), and optical properties of the camera (e.g., maximum view angles to each side of the centre of view). Some or all of these parameters may vary throughout strip-transect surveys in response to the locations and behaviours of the target organisms, and changes in the oceanographic (e.g. current) and seabed (e.g. vertical relief) environments. For example, the camera may be pitched toward the seabed to improve the detection of cryptic benthic invertebrates, or directed more horizontally to observe fishes that are relatively conspicuous and located above the seabed. Over soft, low-relief seabed, an ROV may be navigated close to the seabed, whereas, over high-relief rocky seabed, greater altitude may be necessary to avoid damaging the vehicle, tangling its umbilical, or harming sensitive benthic fauna (e.g., corals and sponges). Nevertheless, when conducting visual surveys with downward- or oblique-facing cameras, transect widths are often estimated infrequently, assumed to be constant within and among surveys, or both (e.g., Adams *et al.*, 1995; Butler *et al.*, 2006; Rooper *et al.*, 2012), which could bias estimates of density and abundance.

To measure objects on or above the seabed and quantify sampled seabed area, oblique-angle still images may be analyzed using a perspective grid (Wakefield and Genin, 1987) or obtained from images collected by a camera with a laser-caliper system using laser projection photogrammetric techniques (Caimi *et al.*, 1993, 1987; Kocak *et al.*, 2004), perhaps implemented in image analysis software (e.g., 3Beam Quantitative Measurement Software or QMS, Green Sky Imaging, LLC). In either case, the techniques may require specialized hardware, proprietary software and storage of voluminous video data. Estimates from image analysis software may be erroneous when one or more laser spots cannot be accurately detected, and must be laboriously identified and corrected by an analyst. The ability to automate measurements of transect width using frequent estimates of camera orientation from calibrated auxiliary sensors and known camera viewing angles would greatly reduce analysis time and cost, and improve estimates of the sampled area during visual surveys in complex seabed types where transect width may vary frequently.

The objectives of this study were to: i) evaluate analytical methods that provide frequent estimates of transect length and width to reduce potential uncertainty in estimates of the sampled area during visual transect surveys; and ii) examine the potential effects of varying seabed relief on those estimates. To accomplish these objectives, we compare: i) the accuracy and precision of distance estimates using a DVL and USBL during ROV transects along submerged pipeline features of known length; ii) estimates of transect width and sampled area derived using: a) parallel-laser metrics and b) measures of the camera pitch, altitude, and viewing angle during a visual survey of cowcod (*Sebastes levis*) off southern CA; iii) estimates of transect width – measured using camera pitch, altitude, and viewing angle – across various seabed types encountered during the cowcod survey; and iv) estimates of sampled area using a range of constant transect widths and those estimated from frequent measures of transect width using: a) parallel-laser metrics and b) camera orientation.

Methods

Transect distance estimation

The Point Loma Ocean Outfall, a 7.2-km long, submerged wastewater-outfall pipeline near San Diego, CA (Figure 1), is constructed from 6.01-m long sections of concrete pipe, joined end-to-end. Manholes along the pipeline mark several shorter section groups (294.49–306.51-m long, depending on the number of pipe sections). The lengths of each concrete pipe section and section group are accurately known (personal communication; M. Kelly, City of San Diego) and were used as references to calibrate transect-distance estimates. A 1520.53-m portion of the pipeline, between manholes 8 and 13, was surveyed three times using a custom high-definition high-voltage ROV (HDHV-ROV; National Marine Fisheries Service, Southwest Fisheries Science Center) deployed from the vessel *Outer Limits* (Figure 1). Depth along the surveyed portion of the pipeline increased with distance from shore, 75–88 m.

The ROV system included a high-definition (HD) digital video camera (Mini Zeus with 1080 interlaced lines of resolution and a 10X optical zoom, Insite Pacific) mounted on a variable-pitch tray with a rotary position sensor (SS131 Feedback Sensor, SIDUS Solutions, Inc.), a DVL (1200 kHz Workhorse Navigator, Teledyne RD Instruments; speed-over-bottom accuracy $= \pm 0.3$ cm s^{-1} at ± 10.0 m s^{-1}), a USBL acoustic positioning system (TrackLink 1500HA, LinkQuest, Inc.; slant range accuracy $= \pm 0.20$ m, positioning accuracy $= 0.25^{\circ}$ or $\pm 0.5\%$ of slant range), and a differential global positioning system (dGPS, CSI Wireless dGPS MAX). The HDHV-ROV also included a parallel laser-caliper system consisting of two high-intensity, narrow-beam lasers (wavelength $= 635$ nm, power $= 15$ mW) spaced 20 cm apart and centred relative to the camera axis. All data were indexed by time and logged synchronously every 2 s using the navigation software (WinFrog, Fugro Pelagos, Inc.). The heading, pitch, roll, and heave of *Outer Limits* was measured using a Meridian Attitude and Heading Reference System (MAHRS, Teledyne TSS) and used by the USBL system to compensate for vessel motion when estimating the location of the ROV. The integrated navigation software used to estimate the geographic position of the ROV, was configured using the accuracy specifications of the DVL and USBL system, and the Kalman filter (0.10, unitless), speed filter (20, unitless), and range gate (20 m) settings recommended in the software documentation. After installation, the USBL transponder beacon was deployed from the bow and each

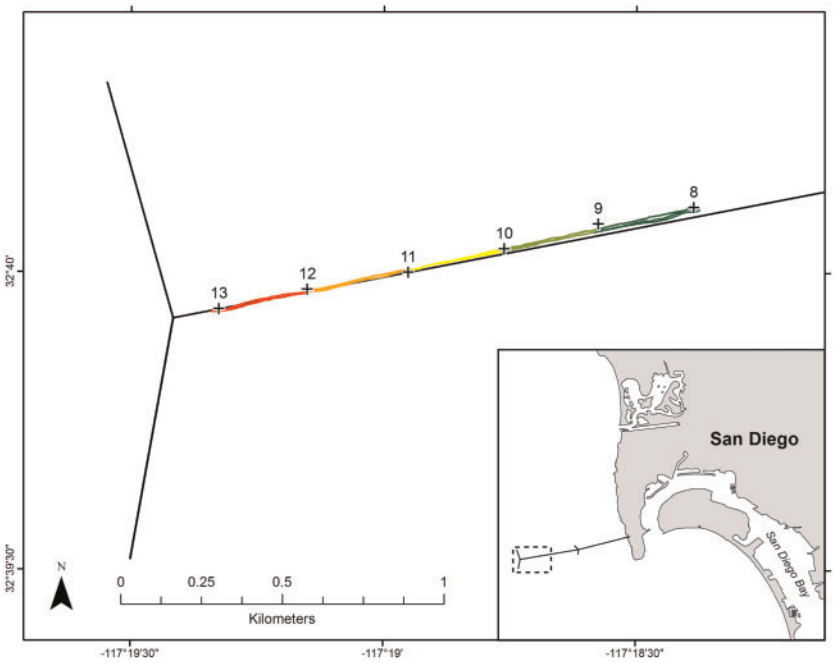

Figure 1. Map of the Point Loma Ocean Outfall survey area near San Diego, California (zoomed area indicated by dashed line in map inset). Three remotely operated vehicle (ROV) transects, represented by the Kalman-filtered geographic positions from the ultra-short baseline (USBL) acoustic system, are plotted and symbolized by pipeline section groups (colored segments). The locations of the manholes that divide the outfall pipeline into five smaller pipeline sections are also shown (numbered crosses).

side of the stern to identify any possible sensor alignment errors. The tether was secured at 5-m intervals to a ~70-kg cylindrical weight suspended from a steel cable to reduce drag on the ROV. A ~30-m length of the tether remained unsecured, which allowed the ROV to move freely around the weight while limiting the horizontal distance between the ROV and the USBL transceiver. All ROV data were indexed by time and logged synchronously every 2 s using the navigation software.

Three replicate transects were conducted in alternating directions, beginning inshore (near manhole 8), by three experienced ROV pilots. For each transect, distance (d) along each pipe section, section group, and the entire pipeline between manholes 8 and 13 was estimated using the DVL (d_{DVL}, m) and USBL (d_{USBL}, m), where d_{DVL} is the sum of i incremental distances (d_{DVL_i}, m) from the product of incremental ROV speed (s_i, m s^{-1}) and the time interval ($t = 2$ s) between speed estimates (i.e., $d_{DVL_i} = s_i * t$); and d_{USBL} is the sum of i incremental Euclidian distances (d_{USBL_i}) between sequential geographic positions of the ROV (northing and easting in the projected Universal Transverse Mercator Zone 11 North coordinate system) estimated every 2 s from the dGPS location of the vessel and the slant range and bearing from the USBL transceiver to the ROV. The Kalman filter was purged at the beginning of each transect. The time when the paired lasers intersected each section and manhole was logged by an observer using the navigation software and used to determine the length of each measured feature. A CTD was cast at the onshore and offshore end of the surveyed area to estimate sound speed versus depth, which could affect USBL performance.

The accuracies of d_{DVL} and d_{USBL} were measured as the difference (Δd_{DVL} and Δd_{USBL}, respectively; %) between the distance estimates and the known length of each feature (L). The precisions of d_{DVL} and d_{USBL} were measured as the coefficients of variation (CV, %) of replicate estimates. Speed, distance, and position data were plotted and visually examined for outliers; two unusually large estimates of d_{USBL_i} ($d_{USBL_i} > 20$ m, $\bar{d}_{USBL_i} = 0.88$ m, $n = 5332$ distance estimates) were manually removed and replaced using linear interpolation. No additional smoothing or filtering was applied to ROV position data. Distance estimates using both methods (d_{DVL} and d_{USBL}) were compared to each other (paired t-test, $\alpha = 0.05$) and to the known length of the each section, section group, and entire pipeline (one-sample t-test, $\alpha = 0.05$).

Transect width estimation

A visual strip-transect survey of cowcod (*Sebastes levis*) was conducted throughout the Southern California Bight (Figure 2) using the HDHV-ROV deployed from *Outer Limits* (Stierhoff *et al.*, 2013). The survey comprised 166 transects with similar length ($\bar{d}_{DVL} = 446$ m, CV = 25%) and duration (mean = 27 min., CV = 23%) that spanned seabed with varying depth (nominally 70 to 300 m), slope, surficial geology (i.e. sediment type, grain size distributions and consolidation), and vertical relief. This survey provided a large data set from which estimates of transect width could be estimated and compared among analysis methods and diverse seabed conditions.

Camera pitch (θ, °; negative below horizontal) was estimated from the pitch angle of the ROV (measured by the DVL; accuracy = ±0.5° up to ±15°) plus the angle from the rotary position sensor. The in-water viewing angles of the video camera vary with zoom. The relationship between camera zoom (indicated by a 0–1 V DC output) and horizontal viewing angle (β,°) was

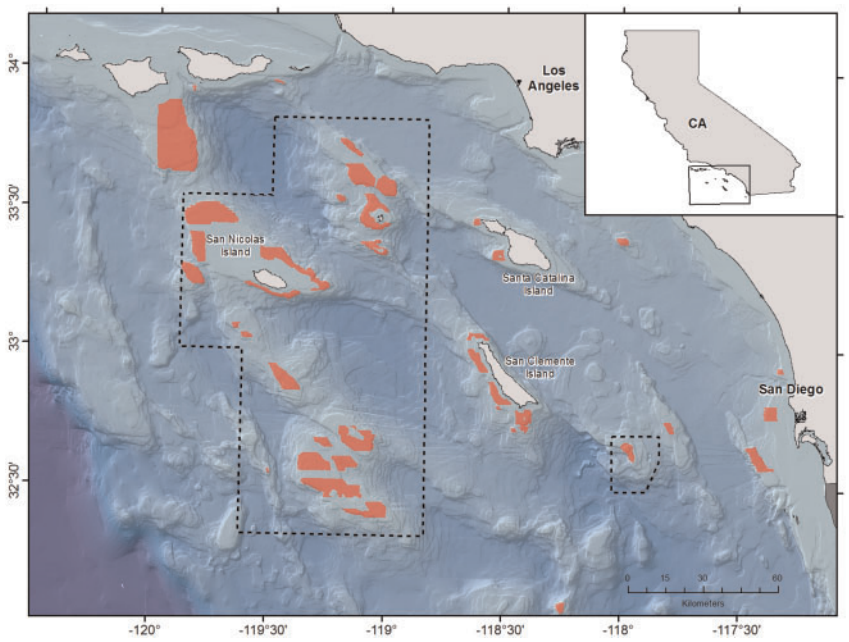

Figure 2. Map of areas sampled (shaded polygons) during the remotely operated vehicle (ROV) survey of cowcod (*Sebastes levis*) habitat in southern California. Depth within areas sampled ranged from 70-300 m. The dashed boxes indicate the extent of the Cowcod Conservation Areas (CCAs).

empirically estimated throughout the zoom range in a seawater tank (Demer *et al.*, 2015) by measuring the viewable width (w, m) of a calibrated grid mounted perpendicular to the camera lens at a fixed distance (R, m):

$$\beta = 2{*}tan^{-1}\left(\frac{0.5w}{R}\right). \quad (1)$$

The horizontal viewing angle of the camera ranged from 2.3° at full-zoom to 74° full-wide, respectively. During the survey, the camera was zoomed slightly (0.06 V) for a horizontal viewing angle of 63°. All HD video was recorded on digital video cassette (HDV, 1080i) tape. Compressed video for QMS analysis was captured using a compact video server (COMCAM-10/BNC microserver, ComCam International) and stored to a hard disk drive.

Using QMS, transect width (i.e., the total width of the video image; w_{QMS}, m) was estimated from compressed video images using the set distance between the parallel laser beams, the measured distance between the laser dots on the seabed (pixels), and the measured width of the image (pixels). The QMS algorithm uses blob analysis on binarized image pixels (Haralick *et al.*, 1987) in the red colour band of each image to detect the centroids of the laser dots on the seabed. An analyst then reviewed the detections, manually marked or adjusted missing or erroneous detections, and re-estimated w_{QMS}. Values of w_{QMS} were estimated every 20 s, resulting in approximately 70 estimates of incremental transect width per transect. QMS can detect lasers every 1 s; however, a preliminary analysis of three transects over low-, medium- and high-relief seabeds, indicated that the estimates of transect width at increasingly greater 1-s intervals provided similar results (i.e., total transect area within ±2.5% of the estimate measured at a 1-s interval) up to ~20 s while reducing the analysis time 20-fold (K. Stierhoff, unpublished data). Values of w_{QMS} were linearly interpolated to match d_{DVL_i} estimated every $i = 2$ s, yielding incremental transect widths (w_{QMS_i}, m) that were assumed to be constant over each 20 s interval.

Incremental measures of camera pitch (θ_i,°) and altitude above the seabed (A_i, m), measured every 2 s and smoothed using a 30-s moving average, were used to calculate slant range from the camera lens to the seabed (R_i, m) (Figure 3):

$$R_i = \left|\frac{A_i}{sin(\theta_i)}\right|. \quad (2)$$

Then, incremental values of transect width were alternatively estimated from the camera parameters (w_{C_i}, m) using the empirical estimate of the in-water, horizontal video-camera viewing angle (β) as:

$$w_{C_i} = 2{*}R_i{*}tan\left(\frac{\beta}{2}\right). \quad (3)$$

When $\theta \geq 0$, R equals infinity (i.e., the centre axis of the camera never intersects the seabed) and w and a may not be computed. Also, R eventually exceeds the maximum viewing range of the camera ($R_{\max}$, estimated as 6 m in this study) either when R is greater than the portion of the seabed that is illuminated by the ROV's lights, or when $\theta = -90°$ and A exceeds $R_{\max}$. In such cases, R_i was set equal to $R_{\max}$ to compute w_{C_i}.

Finally, incremental values of sampled area from QMS (a_{QMS_i}, m^2) and the camera parameters (a_{c_i}) were estimated as the product of d_{DVL_i} and $w_{QMS_{i-1}}$ or $w_{C_{i-1}}$, and total transect area (a_{QMS} and a_C) was estimated for each transect as the sum of a_{QMS_i} or a_{C_i}, respectively. To examine potential bias in biomass-density estimates resulting from the assumption of constant transect width, the total area sampled during the cowcod survey ($a_{QMS_{tot}}$ and $a_{C_{tot}}$, m^2) was estimated as the total distance surveyed (d_{DVL}) multiplied by estimates of $\bar{w}_{C_i}$ and $\bar{w}_{QMS_i}$ for individual transects

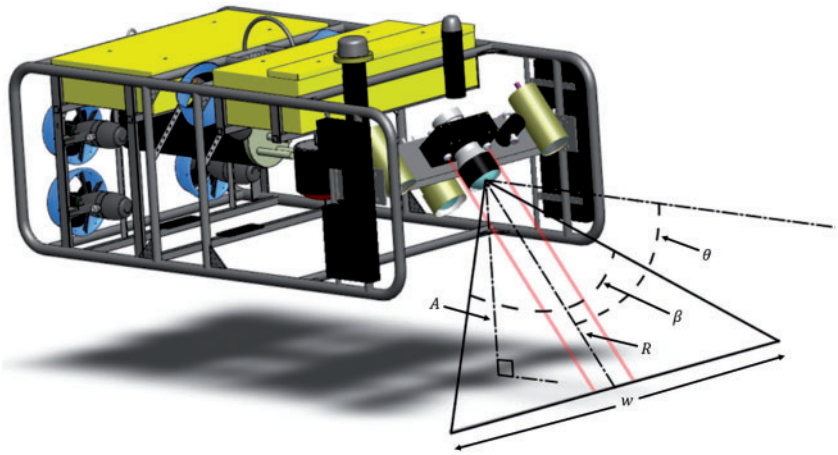

Figure 3. A model representation of the high-definition high-voltage remotely operated vehicle (HDHV-ROV). Transect width (w_{QMS}) is estimated from the spots on the seabed from two parallel lasers, one mounted on each side of the video camera. The parameters used to estimate w_C from the camera altitude (A), pitch (θ), slant range (R), and horizontal in-water viewing angle (β) are also shown.

Table 1. Mean ($\bar{d}$, m), coefficient of variation (CV(d), %), and percent error (Δd, %) of distances estimated from ROV speed (d_{DVL}) and position (d_{USBL}) relative to the known length (L) of reference features.

Feature	Group	n	L	$\bar{d}_{DVL}$	CV(d_{DVL})	Δd_{DVL}	$\bar{d}_{USBL}$	CV(d_{USBL})	Δd_{USBL}
Section	–	741	6.01	6.06	12.7	0.8	6.31	13.1	5.0
Section group	8–9	3	306.51	303.88	0.4	−0.9	316.78	1.5	3.3
	9–10	3	294.49	290.77	0.1	−1.3	308.81	5.3	4.9
	10–11	3	306.51	304.45	0.4	−0.7	313.58	0.4	2.3
	11–12	3	306.51	303.11	0.3	−1.1	313.77	0.5	2.4
	12–13	3	306.51	302.39	0.4	−1.3	316.09	0.4	3.1
Pipeline	–	3	1520.53	1504.61	0.1	−1.0	1569.03	1.1	3.2

Negative and positive values of Δd are under- and over-estimates of L, respectively.

during that survey. Bias (Δa_{QMS} and Δa_C, %) was measured as the difference between the estimates of a_{tot} derived using mean transect widths ($\bar{w}_{QMS_i}$ and $\bar{w}_{C_i}$), and using incremental widths (w_{QMS_i} and w_{C_i}) measured every 2 s or 20 s.

Transect width versus seabed type

To examine the potential effects of seabed morphology and relief on sampled area estimates, each estimate of w_{C_i} was assigned a primary seabed classification (the primary seabed class comprises >50% of the seabed area) following Stein et al. (1992). Seabed classes were based on the particle or feature size: mud (clay to silt; <0.06 mm), sand (0.06-2 mm), pebble (2-64 mm), cobble (64-256 mm), boulder (256-3000 mm); and reef complexity (i.e. the size of cracks and crevices in the seabed that may provide refuge to groundfishes): low (<0.25 m vertical relief; e.g., pavement) and high (>0.25 m vertical relief, Greene *et al.*, 1999).

All computations were conducted using base functions in R (R Core Team, 2013). All figures were produced using the R package *ggplot2* (Wickam, 2009) or ArcGIS v10.2 (Esri, Inc.).

Results

Transect distance estimates

The distance calibration study was conducted under mostly ideal conditions with light wind (< 5 kt) and calm seas (swell <1 m and wind waves <0.3 m). Profiles of temperature, salinity and sound speed differed insignificantly between the inshore and offshore portion of the pipeline and throughout the day. The harmonic-mean sound speed, from the surface to the seabed, was 1505.5 m s^{-1} onshore and 1507.1 m s^{-1} offshore.

Estimates of d_{DVL} and d_{USBL} were similarly precise, but d_{USBL} was less accurate and positively biased compared to d_{DVL}. For individual pipe sections (L = 6.01 m, n = 741 sections), $\bar{d}_{DVL}$ was 6.06 m ($\Delta\bar{d}_{DVL}$ = 0.8%, CV = 12.7%) and $\bar{d}_{USBL}$ was 6.31 m ($\Delta\bar{d}_{USBL}$ = 5%, CV = 13.1%) (Table 1). For longer pipeline section groups (L = 294.49-306.51 m, n = 15 section groups), $\Delta\bar{d}_{DVL}$ was −1.1% (−1.3 ≤ $\Delta\bar{d}_{DVL}$ ≤ -0.7%) and $\Delta\bar{d}_{USBL}$ 3.2% (2.3 ≤ $\Delta\bar{d}_{DVL}$ ≤ 4.9%) (Table 1). Over the entire pipeline (L = 1520.53, n = 3 transects), $\bar{d}_{DVL}$ was 1504.61 m ($\Delta\bar{d}_{DVL}$ = −1.0%, CV = 0.1%) and $\bar{d}_{USBL}$ was 1569.03 m ($\Delta\bar{d}_{USBL}$ = 3.2%, CV = 1.1%) (Table 1). For both methods, accuracy varied little with feature length, but precision increased (i.e. CV decreased) with feature length. For features of all lengths, estimates of d_{DVL} and d_{USBL} were significantly different from each other ($p < 0.05$) and also from the known length of the feature ($p < 0.05$).

Transect width estimation

Measured using camera pitch, altitude, and optical properties, and calculated using equations (2) and (3), $\bar{w}_{C_i}$ throughout the entire cowcod survey was 4.07 m (CV = 31.8%, n = 117,826 transect increments) (Figure 4a). Measured using parallel-laser dots, QMS software, and approximately 80 h of data processing and critical review (~30 min of analysis per transect, n = 166 transects), $\bar{w}_{QMS_i}$ for the same number of increments was 4.19 m (CV = 31.9%) (Figure 4a). A broad range of $\bar{w}_C$ (1.74 ≤ $\bar{w}_C$ ≤ 6.07 m) and

$\bar{w}_{QMS}$ ($1.94 \leq \bar{w}_{QMS} \leq 5.93$ m) were observed among all transects. Estimates of a_C and a_{QMS} are significantly positively correlated ($r^2 = 0.81$, $p < 0.01$, Figure 5), indicating that both methods provide similar estimates of a. The bias in estimates of sampled area (Δa_{tot}, %) ranged from -59.9 - 45.4% across the range of $\bar{w}_C$ and $\bar{w}_{QMS}$ observed among all transects (Figure 4b). Bias was similar between the two methods used to estimate width, and was minimized when the $\bar{w}_C$ or $\bar{w}_{QMS}$ used to calculate a_C and a_{QMS} approximated $\bar{w}_{C_i}$ and $\bar{w}_{QMS_i}$.

Transect width versus seabed type

The most common seabed classes encountered, based on a total transect area within each class, were sand and boulder. Large amounts of cobble and high-relief reef were also encountered (Figure 6a). The $\bar{w}_{C_i}$ generally increased with seabed relief, from 2.82 m (CV = 35.9%) over mud to 4.49 m (CV = 25.4%) over boulders (Figure 6b). Correspondingly, mean camera altitude ($\bar{A}_i$) also increased with seabed relief, from 0.47 m (CV = 81.9%) over mud to 1.72 m (CV = 43.7%) over high-relief reef (Figure 6c). The mean camera pitch ($\bar{\theta}_i$) for each transect ranged from 16 to 40°, but did not vary substantially with seabed relief (Figure 6d).

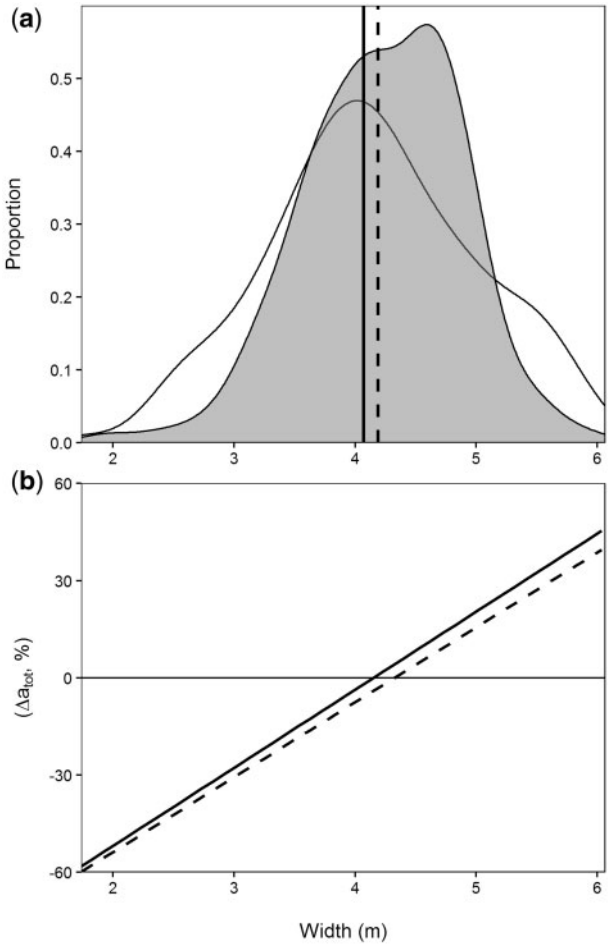

Figure 4. The distribution of mean transect widths estimated from the pitch, altitude, and horizontal viewing angle of the camera ($\bar{w}_{C_i}$, m; unshaded area) and QMS ($\bar{w}_{QMS_i}$ m; gray-shaded area) (n = 166 transects, panel a). The solid and dashed vertical lines indicate the overall mean widths ($\bar{w}_C$ and $\bar{w}_{QMS}$, respectively) across all transects. Bias (Δa_{tot}, %) of area estimates across a range constant mean transect widths relative to area estimated from w_{C_i} (solid line) and w_{QMS_i} (dashed line) measured every 2 s and 20 s (panel b).

Discussion

Estimates of transect distance measured using both speed- and position-based methods were acceptably accurate and precise. Both methods produced distances within 5% of the known feature length, but estimates based on ROV speed were more accurate (within 1%) and slightly more precise than those from position estimates over distances of metres to kilometres. The accuracy of both methods remained relatively constant over the range of distances, while precision increased over greater distances.

The accuracy of any USBL system may be affected by sea state and range to the vehicle, and therefore: water depth; the location of the vehicle relative to the transducer beam pattern; the variability of sound speed versus depth, distance, and time; acoustic interference from bubbles generated by the vessel or weather conditions; uncompensated vessel motion; suboptimal configuration of the tracking and navigation software parameters (e.g., sensor offsets, speed filters, and instrument inaccuracies); or a combination of these factors. This study was conducted under calm sea conditions in relatively shallow water, therefore minimizing the negative effects of bubbles, vessel motion and range on the accuracy of the position estimates. In this study, sound speed did not vary significantly versus depth and distance, but environmental conditions could affect USBL performance over longer periods. The directional transducer was mounted on the starboard rail, forward of the propellers, to minimize any cavitation noise. Sensor offsets were carefully measured and navigation software parameters were configured to the manufacturer's recommended settings for an ROV system using a USBL with a DVL. Tests of the USBL system after the installation did not identify any apparent angular alignment errors. The use of a weight, which

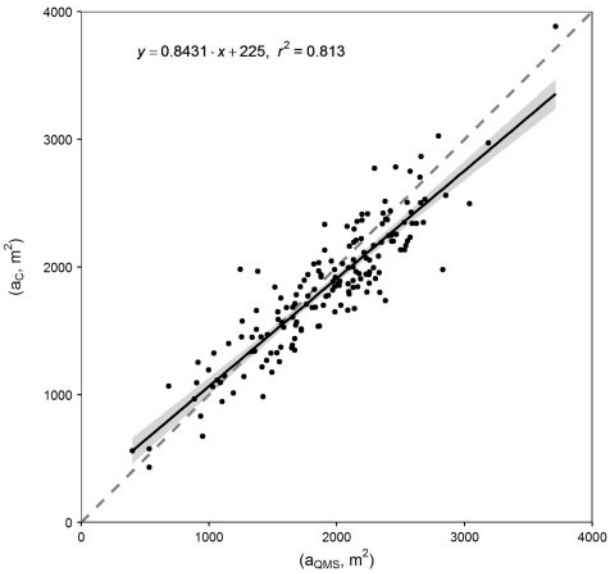

Figure 5. A regression of total transect-area estimates from area estimated by QMS software algorithms (a_{QMS}, m^2) on total transect-area estimates from the pitch, altitude, and horizontal viewing angle of the camera (a_C, m^2; $n = 166$ transects) during the survey of cowcod habitat near southern California. For comparison with the regression equation (solid line), the dashed diagonal line has a slope of 1 and y-intercept of 0. The shaded area indicates the standard error.

minimized the distance from the ROV to the USBL transceiver, should have minimized any systematic errors caused by the potential misalignment of the USBL system sensors, which increase proportionally with range (Opderbecke, 1997). Despite the benign conditions and careful instrumentation setup, the distance estimates from USBL positions were less accurate and precise than those from DVL speed. However, the USBL results may be improved by calibrating the USBL system with the WinFrog navigation software, which was not possible during this study due to logistical constraints. Irrespective of its utility for estimating distance and sampling area, USBL systems remain a critical tool for vessel tracking and navigation during underwater surveys.

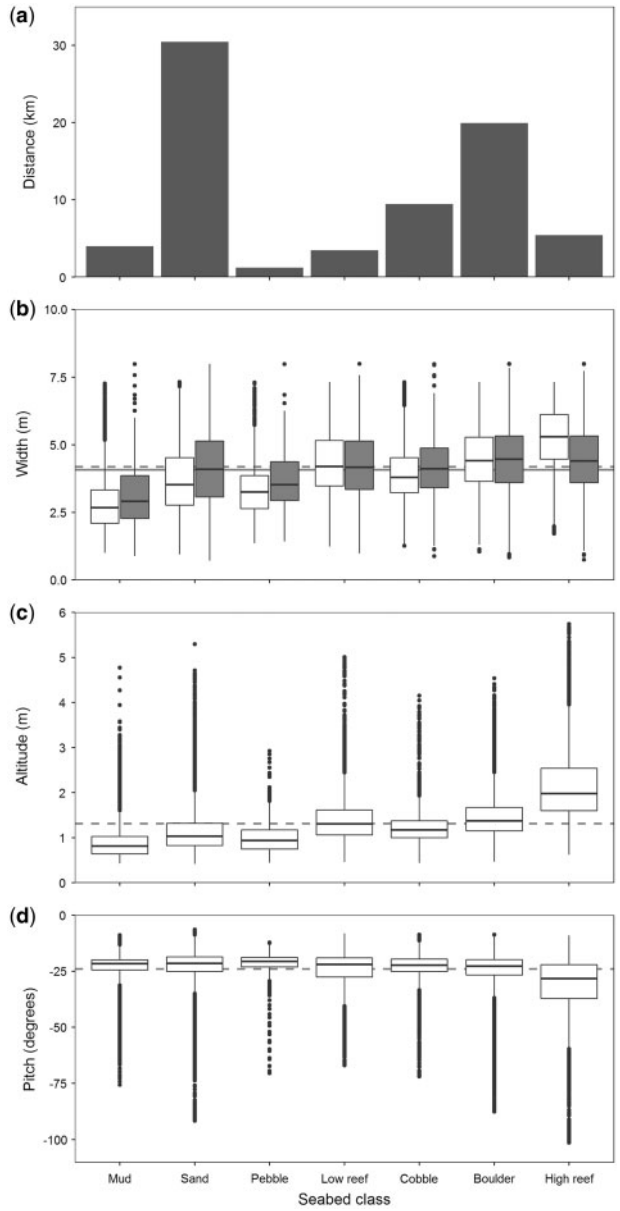

Figure 6. The total transect distance in each primary seabed class (km; panel a), and box and whisker plot of transect width estimated using camera parameters (w_{C_i}, m; white boxes, panel b) and laser metrics (w_{QMS_i}, m; gray boxes, panel b), camera altitude (A_i, m; panel c), camera pitch (θ_i, degrees below horizontal; panel d) in each primary geological seabed class during the cowcod survey. Upper and lower hinges represent the first and third quartiles (the 25th and 75th percentiles), and the whiskers represent 1.5 times the interquartile range. Values outside the whiskers are outliers and plotted as points. The solid and dashed lines in panel b) indicate $\bar{w}_{C_i}$ and $\bar{w}_{QMS_i}$. The dashed horizontal lines in panels c) and d) indicate the mean value across all seabed classes.

The two methods used to measure transect width yielded similar estimates of the total sampled area. The estimates of transect width using the image-based laser-caliper method are laboriously obtained, even when facilitated with QMS software under conditions where the detection algorithm had few errors. Erroneous results from the QMS were more common when the lasers and seabed were of similar colour (e.g., rocks encrusted with calcareous algae); when underwater objects (e.g., kelp) block the laser spot; when one or both lasers reflect off suspended particles; or when a coincident spot from a third crossing laser, often used to estimate the range to the seabed, causes saturation of the image-pixel intensities, which further increased analysis time and effort. In contrast, similar estimates of transect width are more easily estimated from measures of the camera pitch, altitude, and optical properties, facilitated by, in this example, a custom script and open-source software, and is not susceptible to many of the challenges faced by QMS. Laser-caliper systems remain common visual survey tools and may be used to validate our method for estimating transect width (w_C) and area (a_C) on other platforms.

Several factors may affect camera orientation, and thus estimates of transect width. In this study, transect width varied with camera altitude, which was modulated by the vertical relief of the seabed. Furthermore, mean camera pitch may be adjusted for the target species and survey objectives, thereby affecting estimates of width and area. For example, the mean camera pitch ($\bar{\theta}$) was -24° and mean camera altitude ($\bar{A}$) was 1.32 m while surveying cowcod, which are large-bodied, conspicuous, and often reside in high-relief habitats, resulting in a mean transect width ($\bar{w}_{C_i}$) of 4.07 m (CV = 31.8%; this study). For comparison, $\bar{\theta}$ was -40°, $\bar{A}$ was 1.70 m, and $\bar{w}_{C_i}$ was 3.43 m (CV = 49.7%, n = 48 transects) while surveying white abalone (*Haliotis sorenseni*; Stierhoff *et al.*, 2014), which are cryptic and attached to the seabed. Therefore, transect width estimates are likely different within and among surveys, even when conducted using the same platform, especially if the target species differ in appearance, behaviour, or habitat, or when surveying in areas where seabed relief changes.

Given the effort necessary to frequently estimate transect width using image-based methods, it may be tempting to estimate $\bar{w}$ for a subset of transects and assume a constant transect width within and among surveys. However, it is unknown whether the selected subset of transects is representative of other transects. In this study, the sampled area estimated using the mean width across 166 transects would have closely approximated the area estimated from w_C measured every 2 s. However, significant bias in sampled area, and thus animal density, may have occurred had the subset of transects used to compute mean transect width been selected from either tail of the transect-width distribution. The methods described for the frequent estimation of transect width from camera metrics should minimize bias associated with changes in camera orientation.

Optical properties of the camera may also affect estimates of transect width. As seen in equation (3), the transect width and thus the area sampled are directly proportional to $tan\left(\frac{\beta_i}{2}\right)$. The manufacturer's specifications for the in-water horizontal viewing angle may be inaccurate and should be measured. For example,

the camera on the HDHV-ROV, the empirical estimate of $\beta = 74°$ was 13.0% less than the manufacturer's specification of 85°. In this case, use of the nominal value for β would result in the overestimation of the sampled areas by 17.8%, thereby underestimating animal density, abundance, and biomass.

Conclusion

Transect distances and widths that are inaccurate, imprecise, or both contribute uncertainty to estimates of optically-sampled areas and animal populations. To minimize this uncertainty, it is essential to frequently, accurately, and precisely estimate distance and width within and among transects, between surveys, and among survey platforms. These estimates may be readily generated using a DVL and attitude sensor data collected during visual surveys. It is advisable, if possible, to calibrate the sensors and methods used to estimate sampled areas using reference standards.

Acknowledgements

We thank Ben Hong for his contributions to early 3Beam QMS analyses. We also thank Mike Kelly, City of San Diego, for providing essential information about the Point Loma Ocean Outfall. John Butler designed the pipeline calibration survey. Critical reviews by George Cutter and two anonymous reviewers greatly improved upon earlier versions of this manuscript.

References

Adams, P. B., Butler, J. L., Baxter, C. H., Laidig, T. E., Dahlin, K. A., and Wakefield, W. W. 1995. Population estimates of Pacific Coast groundfishes from video transects and swept-area trawls. Fishery Bulletin 93, 446–455.

Buckland, S., Anderson, D., Burnham, K., Laake, J., Borchers, D., and Thomas, L. 2001. Introduction to Distance Sampling. Oxford University Press, Inc., New York, NY.

Butler, J., Neuman, M., Pinkard, D., Kvitek, R., and Cochrane, G. 2006. The use of multibeam sonar mapping techniques to refine population estimates of the endangered white abalone (*Haliotis sorenseni*). Fishery Bulletin 104, 521–532.

Caimi, F. M., Blatt, J. H., Grossman, B. G., Smith, D., Hooker, J., Kocak, D. M., and Gonzalez, F. 1993. Advanced underwater laser systems for ranging, size estimation, and profiling. Marine Technology Society Journal 27, 31–41.

Caimi, F. M., Tusting, R., and Hardin, D. 1987. Laser-aided quantitative sampling of the sea bed. MTS/IEEE Oceans '87, 1234–1238.

Demer, D. A., Cutter, J. G. R., Stierhoff, K., and Renfree, J. S. 2015. Two-million-liter tank expands the boundaries of marine technology innovation: National resource available for advancing marine science. Marine Technology Society Journal 49, 87–98.

Greene, H. G., Yoklavich, M. M., Starr, R. M., O'Connell, V. M., Wakefield, W. W., Sullivan, D. E., McRea, J., *et al.* 1999. A classification scheme for deep seafloor habitats. Oceanologica Acta 22, 663–678.

Haralick, R. M., Sternberg, S. R., and Zhuang, X. 1987. Image analysis using mathematical morphology. IEEE Transactions on Pattern Analysis and Machine Intelligence PAMI-9, 532–550.

Jagielo, T., Hoffman, A., Tagart, J., and Zimmermann, M. 2003. Demersal groundfish densities in trawlable and untrawlable habitats off washington: Implications for the estimation of habitat bias in trawl surveys. Fishery Bulletin 101, 545–565.

Kalman, R. 1960. A new approach to linear filtering and prediction problems. Journal of Basic Engineering 82, 35–45.

Keller, A., Horness, B., Tuttle, V., Wallace, J. R., Simon, V., Fruh, E., Bosley, K. L., *et al.* 2006. The 2002 U.S. West Coast Upper Continental Slope Trawl Survey of Groundfish Resources off Washington, Oregon, and California: Estimates of Distribution, Abundance, and Length Composition. U.S. Dep. Commer., NOAA Tech. Memo., NMFS-NWFSC-75: 189 pp.

Keller, A., Simon, V., Horness, B., Wallace, J. R., Tuttle, V., Fruh, E., Bosley, K. L., *et al.* 2007. The 2003 U.S. West Coast Bottom Trawl Survey of Groundfish Resources off Washington, Oregon, and California: Estimates of Distribution, Abundance, and Length Composition. U.S. Dep. Commer., NOAA Tech. Memo., NMFS-NWFSC-86: 130 pp.

Kocak, D. M., Jagielo, T., Wallace, F., and Kloske, J. 2004. Remote sensing using laser projection photogrammetrically aided underwater video system for quantification and mensuration in underwater surveys. IEEE IGARSS '04

Opderbecke, J. 1997. At-sea calibration of a uSBL underwater vehicle positioning system. MTS/IEEE Oceans '97 Vols 1 and 2, 721–726.

O'Connell, V. M., and Carlile, D. 1993. Habitat-specific density of adult yelloweye rockfish *Sebastes ruberrimus* in the eastern Gulf of Alaska. Fishery Bulletin 91, 304–309.

Pinkard, D., Kocak, D. M., and Butler, J. 2005. Use of a video and laser system to quantify transect area for remotely operated vehicle (ROV) rockfish and abalone surveys. MTS/IEEE Oceans '05 3, 2824–2829.

R Core Team. 2013. R: A language and environment for statistical computing. http://www.R-project.org/.

Rooper, C. N., Martin, M. H., Butler, J. L., Jones, D. T., and Zimmermann, M. 2012. Estimating species and size composition of rockfishes to verify targets in acoustic surveys of untrawlable areas. Fishery Bulletin 110, 317–331.

Stein, D. L., Tissot, B. N., Hixon, M. A., and Barss, W. 1992. Fish-habitat associations on a deep reef at the edge of the Oregon continental shelf. Fishery Bulletin 90, 540–551.

Stierhoff, K., Mau, S., and Murfin, D. 2013. A fishery-independent survey of cowcod (*Sebastes levis*) in the Southern CA Bight using a remotely operated vehicle (ROV). U.S. Dep. Commer., NOAA Tech. Memo., NMFS-SWFSC-520: 92 pp.

Stierhoff, K., Neuman, M., and Butler, J. 2012. On the road to extinction: Population declines of the endangered white abalone, *Haliotis sorenseni*. Biological Conservation 152, 46–52.

Stierhoff, K., Neuman, M., Mau, S., and Murfin, D. 2014. White abalone at San Clemente Island: Population estimates and management recommendations. U.S. Dep. Commer., NOAA Tech. Memo., NMFS-SWFSC-527: 25 pp.

Wakefield, W. W., and Genin, A. 1987. The use of a Canadian (perspective) grid in deep-sea photography. Deep-Sea Research Part I: Oceanographic Research Papers 34, 469–478.

Wickam, H. 2009. ggplot2: Elegant graphics for data analysis. Springer, New York.

Yoklavich, M. M., Greene, H. G., Cailliet, G. M., Sullivan, D. E., Lea, R. N., and Love, M. S. 2000. Habitat associations of deep-water rockfishes in a submarine canyon: An example of a natural refuge. Fishery Bulletin 98, 625–641.

Yoklavich, M. M., Love, M. S., and Forney, K. A. 2007. A fishery-independent assessment of an overfished rockfish stock, cowcod (*Sebastes levis*), using direct observations from an occupied submersible. Canadian Journal of Fisheries and Aquatic Sciences 64, 1795–1804.

Handling editor: Richard O'Driscoll